Development and application of the field imaging spectrometer system

TONG Qingxi[1], XUE Yongqi[2], WANG Jinnian[1], ZHANG Lifu[1], FANG Junyong[1], YANG Yide[2], LIU Xue[1], QI Hongxing[2], ZHENG Lanfen[1], HUANG Changping[1]

1. *State Key Laboratory of Remote Sensing Sciences, Institute of Remote Sensing Applications, Chinese Academy of Sciences, Beijing* 100101, *China*;
2. *Shanghai Institute of Technical Physics, Chinese Academy of Sciences, Shanghai* 200083, *China*

Abstract: This paper describes the field imaging spectrometer system (FISS) based on a cooling area CCD, describing its imaging principle, structural design, main technology parameters, and data processing flow. Geometric rectification of the FISS was implemented using precise indoor markers and outdoor measured data. Spectral calibration of the FISS was conducted using self-programmed spectral calibration software which determined the center wavelength and the full width at half maximum of each band. An integrating sphere was used to achieve absolute radiometric calibration of the FISS with less than 5% calibration error for each band. In addition, a look-up table of radiometric calibration coefficients for various measured conditions was generated and various laboratory and field tests were carried out. Crop-weed discrimination, offshore marine environment monitoring, milk discrimination, and estimation of vegetation biochemical information were studied using previously acquired data. The FISS provided successful results for all of the above examples, suggesting its potential application in other fields, including geology, food science, agriculture, forestry, and urban research.

Key words: hyperspectral remote sensing, imaging spectrometer, field imaging spectrometer system (FISS), system design, remote sensing application

CLC number: TP702 **Document code:** A

Citation format: Tong Q X, Xue Y Q, Wang J N, Zhang L F, Fang J Y, Yang Y D, Liu X, Qi H X, Zheng L F and Huang C P. 2010. Development and application of the field imaging spectrometer system. *Journal of Remote Sensing.* **14**(3): 409—422

1 INTRODUCTION

Imaging spectrometry combines traditional two-dimensional (2-D) remote sensing technology and spectroscopy, enabling acquisition of both the images and spectra of objects and thus combining 'an image and a spectrum'. The emergence of ima ging spectrometers has resolved past problems of obtaining either images without spectra or spectra without images (Tong *et al*., 2006; Zhang *et al*., 2005). China's aviation imaging spectrometry industry is now relatively mature, and researchers have made a series of breakthroughs and achievements that place China in an important position internationally in airborne imaging spectrometry (Liu *et al*., 2002).

Data observed by airborne imaging spectrometers can only be used to monitor or evaluate objects from the macro level, with spatial resolution of a few meters to tens of meters (Green *et al*., 1998). Because of the effects of observation scale, angle, and background, the spectra extracted from images are not pure single-feature spectra; this leads to a certain degree of bias in the resulting analysis and applications. To study objects at a micro level, we must increase ground resolutions, reduce background effects, and improve the stability and accuracy of spectral measurements. To promote the further development and improvement of both field spectral measurements and aviation imaging spectrometry in China, the Institute of Remote Sensing Applications and the Shanghai Institute of Technical Physics, both of which belong to the Chinese Academy of Sciences, developed the field imaging spectrometer system (FISS). The FISS is based on the aviation push-broom imaging spectrometer (PHI) also developed in China. In field measurements, the FISS can obtain high-resolution images (spatial resolution up to the centimeter or millimeter scale) of measured targets as well as extract a spectrum curve of any pixel from these images. The FISS both improves the efficiency of field spectral measurements and provides better information and data for analyzing the structure of spectra, decomposing mixtures of spectra, and extracting pure spectra. Compared to spectra by traditional field spectrometers, those obtained by the FISS may be considered pure spectra and will be helpful for studying mixtures of spectra and analyzing the composition and structure of pixels at

Received: 2010-03-04; **Accepted**: 2010-03-11

Foundation: Major Research Equipment Development Project of Chinese Academy of Sciences (Field Imaging Spectrometer System Development); National 863 Key Program (No. 2008AA121102 and No.2008AA121103); National Scientific Technology Support Project (No. 2007BAH15B01).

First author biography: TONG Qingxi (1935—), male, professor and doctoral adviser, academician of Chinese Academy of Sciences, fellow of International Europe and Asia Academy of Sciences. He is an expert in remote sensing technology and application, creating and developing the hyperspectral remote sensing technology and its applications. He has published more than 70 monographs and papers. E-mail: tqxi@263.net

variable spatial scales.

Previous studies have applied field imaging spectrometers to various regions and applications (Borregaard *et al*., 1999; Ye *et al*., 2007). At present, many foreign companies and institutions specialize in the development of such devices, including Spectral Imaging Ltd. (Finland), Resonon Inc. (U.S.), and Surface Optics Corporation (U.S.). However, before the FISS, no field imaging spectrometer based on a cooling area CCD had been developed in China; the FISS thus represents original innovation of a scientific instrument for basic research in remote sensing. In addition, breakthroughs in key technologies that were achieved during development of the FISS may promote advancement in other fields including detector technology, imaging spectrometry, spectroscopic techniques, high-speed data acquisition, and storage technologies, and may enhance independent innovation.

2 DEVELOPMENT AND REALIZATION OF THE FISS

2.1 Basic principle of design

Development of the FISS, using examples from the PHI, focused on improvement or redesign of the imaging system, optical spitting system, and control software. The imaging principle of the FISS is similar to that of the PHI: one direction along the slit forms a spatial line image, while the direction perpendicular to the slit measures the spectrum for each line pixel made by the dispersion component, and another dimension is scanned by the scanning mirror (Fang *et al*., 2009; Li *et al*., 1999).

Fig. 1 shows the imaging principle of the FISS. The front optics image the object line onto the entrance slit plate and then successively through a collimating mirror, making collimated light. A dispersing unit, in which the incident radiation is spread according to wavelength in the vertical direction, and a collective lens finally form an image in the CCD chip. In the image, the spectra of the object line are represented by values in the rows (parallel to the slit; called the spatial axis), while the radiation, within a narrow spectral band received from the line, is found in the columns (dispersion direction; called the spectral axis). The CCD can generate a spectral-spatial image for each object line and, by scanning with the scanning mirror within a certain angle and record rate, spectral data can be continuously recorded to obtain an image cube.

2.2 Structural design

The FISS consists of three main parts: the computer, optical, and electronic systems. The computer system includes hardware (a portable laptop used for real-time monitoring and storing the imaging data and other ancillary data) and software (the program used to operate the FISS and some basic data processing and analysis programs).

The optical systems consist of a scanning mirror, an objective lens, a dispersing unit, and a CCD camera and are the core parts of the FISS. Fig. 2 shows the actual FISS optical systems that have been successfully developed.

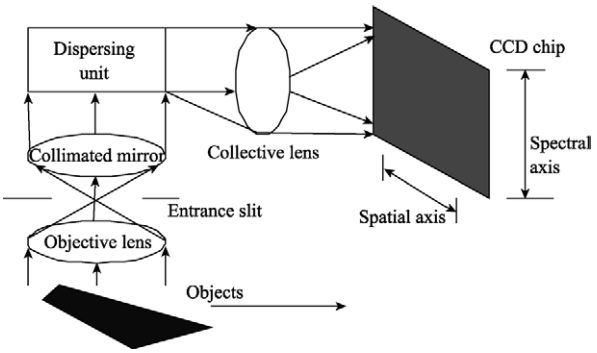

Fig. 1 Basic principle of the FISS

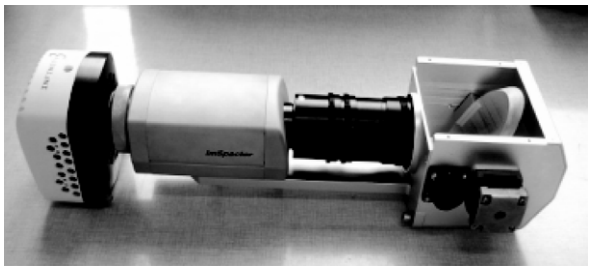

Fig. 2 Photograph of the developed FISS optical systems

The optical systems perform scanning, imaging, dispersion, photoelectric conversion, A/D conversion, and other functions. The scanning mirror, composed of an elliptical reflecting mirror, a stepper motor, and their mechanical framework, is driven by the stepper motor to swing back and forth within a certain angle to achieve imaging of an object in one spatial dimension. The objective lens images objects clearly onto the entrance slit plate laid on the focal plane of the dispersion unit. Together with the objective, the dimensions of the slit determine the field of view. The dispersing unit, using a “prism-grating-prism” (PGP) spectrograph, disperses the light beam from the entrance slit, and then rays with different wavelengths separated by the PGP-element are captured by the focal plane of the CCD camera. The dispersing unit, together with the slit, determines the number of bands and the spectral resolution of the FISS. In the CCD chip (Model INFINITY3-1), the radiation is converted into proportional electrical signals which determine the clarity of the obtained image, i.e., whether it can achieve the spatial and spectral resolution determined by the PGP.

The major components of the electronic systems are the power supply to the CCD camera and the motor control circuits responsible for receiving computer commands to drive the motor, controlling communications between the USB interface and the computer, and taking power from the USB port.

To make field measurements, a multi-use platform was designed that is durable, compact, mobile, flexible, and easy to set-up and dismantle. A high-strength support and spiral arm were designed using a stable triangle form, and a revolving shaft and bolt were used to revolve and fix the spiral arm. The location and angle parameters of the spiral arm are provided by a linear and circular dial. Fig. 3 shows a diagram of the composition of the FISS.

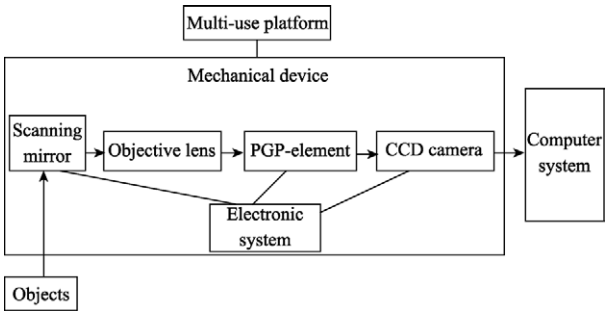

Fig. 3 Composition diagram of the FISS

The multi-use platform consists of a tripod and a precision lever, which are used to carry the optical and electronic systems. The length of the lever can be controlled and measurements can be conducted within a 360° horizontal plane. Precise location information can be provided by using the system together with a high-precision GPS. Fig. 4 presents a schematic diagram and an actual picture of the FISS field measurements.

2.3 Main technical parameters

There are various technical parameters for the FISS, including the spectral range, spectral and spatial resolution, and scanning rate. Table 1 lists the main technical parameters and performance of the FISS.

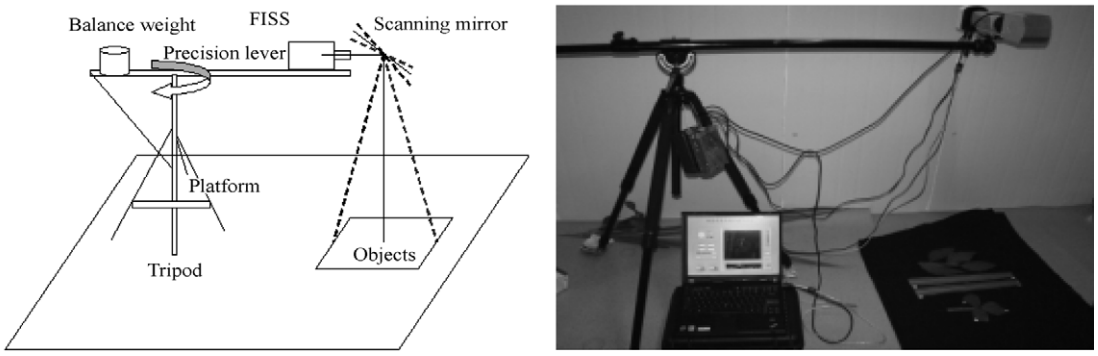

Fig. 4 Schematic diagram and actual photograph of FISS field measurements

Table 1 Main parameters and performance of the FISS

Band number	344
Spectral range /nm	379—870
Spectral resolution /nm	4—7
Space resolution /mm	The maximum is better than 2
Radiance calibration precision in laboratory /%	Better than 5
Imaging rate / (lines/s)	Maximum of 20
Scan field /°	−20—20
Quantitative value /bit	12
Signal to noise	>500 (60% of bands)
Spectral sampling interval /nm	About 1.4

2.3.1 Spectral range and spectral resolution

The spectral range of the FISS depends on the light splitters and the spectral response range of the CCD camera. The spectral response of the CCD sensor is 400–1000 nm, and the spectral response of light splitters (Inspector V9) is 430–900 nm. Thus the FISS spectral range is mainly determined by the spectral range of light splitters. Spectral calibration was conducted using a monochromator in the laboratory. Results show that the FISS responded to the light of the monochromator within 420–860 nm.

The spectral resolution of the FISS is determined by the entrance slit (60 μm width) of the light splitters and the size of the CCD photosensitive component. To meet the required signal to noise ratio, the pixels were merged by 3×3, which reduced the CCD resolution from 1392×1040 to 464×344, where 464 denotes the spatial dimensions and 344 denotes the spectral dimensions, i.e., the FISS has 344 spectral channels. As a result, the photosensitive component size is about 20 μm. Due to the 1 1 imaging mechanism of the CCD, the spectral resolution, expressed as the half-height width of each spectral response curve, depends on the entrance slit.

2.3.2 Spatial resolution

The spatial resolution of the FISS is related to both the parallel and perpendicular directions of the entrance slit. The spatial resolution of the direction parallel to the entrance slit (expressed as Eq.(1)) depends on the size of the imaging unit in the CCD camera focal plane and the focal length of the objective lens:

$$\beta = d/f \tag{1}$$

The spatial resolution of the direction perpendicular to the entrance slit (expressed as Eq.(2)) depends on the width of the entrance slit and the focal length of the objective lens:

$$\alpha = w/f \tag{2}$$

where β is the view angle parallel to the entrance slit, d is the size of the imaging cell, α is the view angle vertical to the entrance slit, w is the width of the entrance slit, and f is the focal length of the objective lens.

2.3.3 Frame rate

The frame rate generally depends on the data transfer rate and the data acquisition mode of the CCD camera. Data are

transported through USB interfaces from the CCD camera in the FISS, with 12-bit data sampling. To avoid image blurring as a result of asynchronization between data acquisition by the flow mode (camera mode) and the stepper motor, the photo mode was chosen for data acquisition. The photo mode means that at each step the stepper motor may issue a synchronous signal to trigger the camera to take a picture. In the photo mode, the frame rate of the CCD camera may be up to 20 lines/s but is often set to 10 lines/s in field experiments.

3 FISS DATA PROCESSING

Before specific application, it was necessary to run a series of processes on the original FISS data including data format conversion, geometric correction, radiometric correction (radiometric calibration), image segmentation, interception and splicing, and other processing techniques for specific applications. Fig. 5 shows a general flow chart of data processing for the FISS.

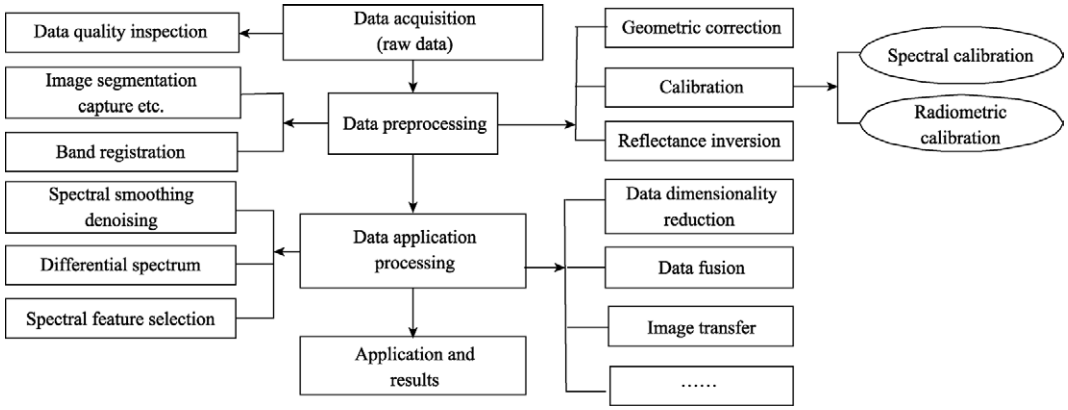

Fig. 5 General flow chart of data processing for FISS

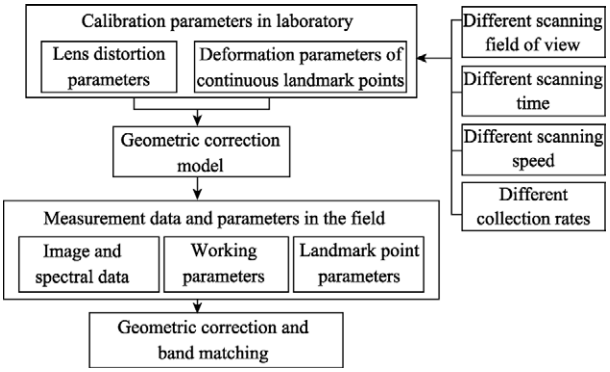

Fig. 6 Flow chart of geometric correction for the FISS

Using the markers above, the system deformation parameters for calibrating FISS data were calculated based on the polynomial geometric correction model.

3.2 Spectral calibration

Using a WDG30-2 monochromator, made by the Beijing Optical Instrument Factory, and the self-developed spectral calibration software, FISS spectral calibration was performed in the laboratory to determine the center wavelengths and full width at half maximum (FWHM) for each spectral channel. The calibration results recorded spectral bandwidths corresponding to different wavelengths and center wavelengths of 344 spectral channels. Table 2 lists the spectral bandwidths corresponding to 420–860 nm that verified a fine spectral response.

Table 2 Spectral channel bandwidths corresponding to 420–860 nm

Range of wavelength/nm	420–470	475–625	630–715	720–820	825–860
FWHM/nm	7	4	5	6	7

3.3 Radiometric calibration

Radiometric calibration of the FISS was achieved by adopting combinations of the absolute radiometric calibration in the laboratory and relative calibration on site. A well-calibrated integrating sphere was used as an indoor light source to fill the entire field of view to obtain absolute radiometric calibration by

3.1 Geometric correction

With the swing of the reflecting mirror within a certain angle range, instead of the movement of a flying platform, the FISS obtains one-dimensional spatial information of surface features that are not imaged at the same time. The differences in imaging distance during scanning by the scanning mirror may create unevenly distributed resolutions among different columns, causing geometric distortion. Moreover, resolutions may also differ among lines because of instability of the scanning mirror. To correct these geometric deformations, it was necessary to measure lens distortion coefficients, establish precise markers, and determine the geometric correction model. To validate and calibrate the stationarity and scanning uniformity of the scanning mirror, continuous markers should be established. The geometric deformation information obtained may also help in controlling the motor. Fig. 6 shows the general flow chart of the geometric correction process for the FISS.

band (Tong *et al*., 2006). By changing the radiance of the integrating sphere (i.e., by controlling the number of bright and dark standard lights within the integrating sphere; total of eight levels), and changing the aperture size of optical lens, integration time, and CCD cooling temperature to meet the application requirements, the quantitative relationship between the entrance radiance at the pupil of the FISS and the digital number was established as follows: $L_e = a \times \mathrm{DN} + b$ (where L_e is the entrance radiance at the pupil, and DN is the digital number value). The values of a and b, which are the calibration coefficients of each band under all kinds of temperature, aperture, and integration time, were computed by linear fitting. In addition, a look-up table for absolute radiometric calibration coefficients of the FISS was built under different measurement conditions. Fig. 7 (a), where the straight line is the linear regression fitted line and the scatters are the actual measured values, shows the calibration results of band 30 (central wavelength of 417.5 nm) under the condition that the optical lens aperture was set to 11, the CCD cooling temperature was 0°C, and the integration time was 5 ms. The abscissa denotes DN values while the ordinate denotes the corresponding entrance radiation. In the calibration coefficient look-up table, the calibration coefficients of band 30 and its calibration accuracy can be found easily (a = 0.058063, b = –0.30929) and the calibration accuracy is 3.6%. Fig. 7 (b) shows the calibration accuracies of 344 spectral channels under the same measurement conditions.

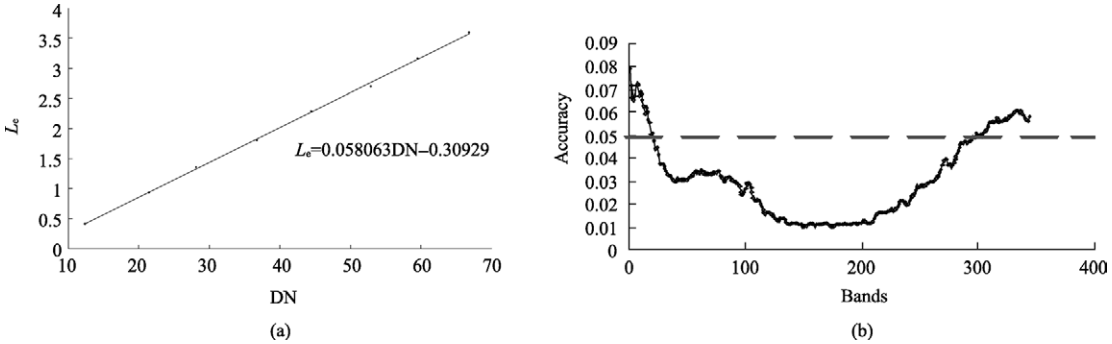

Fig. 7 Absolute radiometric calibration results in the laboratory
(a) Radiometric calibration results of band 30(central wavelength = 417.5 nm); (b) Calibration accuracies of 344 spectral channels with optical lens aperture of 11, CCD cooling temperature of 0°C, and integration time of 5 ms

As indicated in Fig. 7 (b), the radiometric calibration accuracies of most bands are better than 5%, particularly in bands 32–338 (420–860 nm), meeting the requirements of absolute radiometric calibration accuracy in the laboratory.

In the field, relative radiometric calibration of the FISS is achieved with a reference board, i.e., before ground targets are measured the reference board is measured under the same conditions.

4 PRELIMINARY APPLICATION RESULTS OF THE FISS

To obtain various kinds of imaging hyperspectral data and debug the system, many indoor/outdoor measurement tests have been carried out with the FISS prototype. Fig. 8 presents a photograph of the FISS in the field.

Fig. 8 Photograph of the FISS being used in the field

4.1 Indoor spectroscopy experiments with milk

Twelve kinds of milk were purchased from a supermarket, including the Yili, Mengniu, Guangming, and Sanyuan brands. Milk samples were measured in the laboratory by the FISS and by the SVC HR-1024 radiometer (developed by SVC) with a halogen lamp as the light source. To demonstrate the stability, accuracy, and practical performance of the FISS, data obtained simultaneously by the HR-1024 were used as base information. The FISS spectral data were evaluated using spectral angle mapping (SAM), spectral feature fitting (SFF), and binary encoding (BE). Fig. 9 shows milk cube data by the FISS and a continuous spectral curve extracted from one pixel. Fig. 10 shows the evaluation results (SAM, SFF, and BE share 1/3 weight each, and the spectral matching accuracy is over 97%), which indicate that the FISS has good spectral response performance. This promising result provides a theoretical basis for follow-up applied research on the FISS.

In addition, the milk data obtained by the FISS were randomly sampled, with 100 pixel sampled from each kind of milk. These pixels samples were then pre-processed using first-order derivatives and moving averages (Wang *et al*., 2006). Twelve characteristic wavelengths selected by the Wilks' lambda stepwise analysis method were used to discriminate different varieties of milk by the Fisher linear discriminator. The results show overall correct discrimination accuracy of 94.1% for all 12 kinds of milk, with particularly high discriminant accuracies of up to 100% for Mengniu original yogurt and Yili original yogurt.

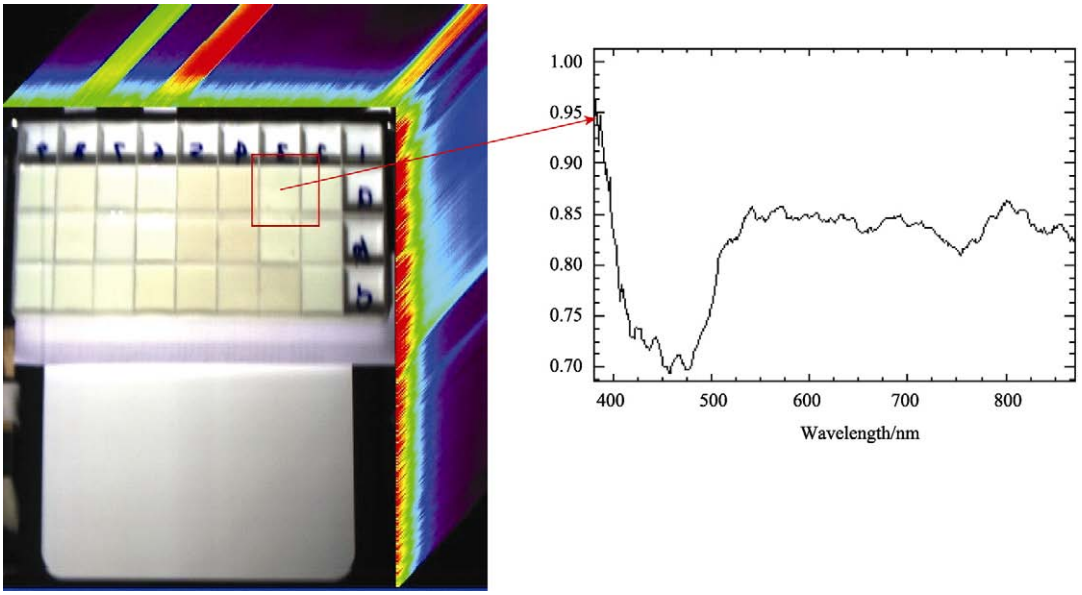

Fig. 9 Milk cube data obtained by the FISS

4.2 Crop-weed discrimination

In-field hyperspectral data were obtained by the FISS for crop-weed discrimination in farmland in Wugezhuang, Beijing Daxing district. After sampling and normalizing the data, crop-weed discrimination was performed using the same method as above (Fisher linear discriminant analysis) (Liu *et al*., In press). When considering each species as a different class, discrimination accuracy reached 85% with eight selected bands. When considering overall weed species as a class, classification accuracy was higher than 91% with eight selected bands. Furthermore, a "red edge" was found to supply much information for discriminating between weeds and crops. Fig. 11 (a) shows crop and weed cube data by the FISS, and Fig. 11 (b) shows the discrimination result.

4.3 Estimating biochemical information for vegetation

Chlorophyll and nitrogen are important biochemical parameters indicating the biochemical status of plants and provide important information for site-specific application of fertilizers.

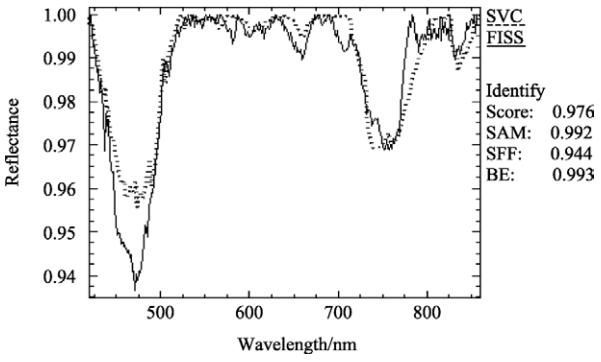

Fig. 10 Spectral matching between the FISS and SVC HR-1024

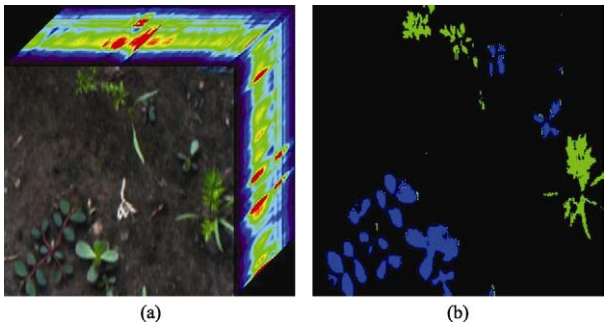

Fig. 11 Crop-weed discrimination
(a) Cube data of crop-weed; (b) Discrimination result

In August 2009, using the FISS and a traditional point-record spectrometer (ASD), hyperspectral data of 102 soybean leaf samples were obtained in the Huanjiang Experimental Station of the Karst Ecosystem, Chinese Academy of Sciences. After preprocessing soybean spectral data and removing an abnormal sample, the soybean leaf chlorophyll and nitrogen content estimation model was established. Results show that the FISS data can be used to quantify inverse biochemical parameters of soybean leaves. The prediction accuracy was higher than 95% using a partial least-squares regression (PLSR) model, based on data mixed with image deviation and mean data. Compared with the ASD data, the FISS data provided higher prediction accuracy for chlorophyll and nitrogen content. Table 3 shows the inverse results based on the principal component regression (PCR) and PLSR model; prediction accuracies were 33% and 42% higher using the FISS data than by using the ASD data, respectively.

Table 3 Comparison of estimation results based on FISS data and ASD data

	FISS		ASD	
	RMSE (prediction)	R^2	RMSE (prediction)	R^2
PCR	0.272332	0.873925	0.405452	0.720781
PLSR	0.236337	0.95001	0.406416	0.84673

4.4 Offshore marine environment monitoring

An offshore marine environment experiment was carried out with the FISS on 28 November 2009. The FISS was mounted on a car and elevated over 30 m high. High-resolution imaging data of the offshore marine environment in Qingdao were captured with the FISS. Many useful hyperspectral data could be obtained by analyzing these data, such as the chlorophyll distribution of seawater, seawater turbidity, and marine pollution and distribution. Thus the FISS may be helpful for quantitatively analyzing marine environments. These initial analyses indicate that the FISS is effective for the examples given above and has important application value.

5 CONCLUSION AND PROSPECTS

The self-developed field imaging spectrometer system (FISS) is able to measure spectra while acquiring high-resolution images of objects and achieving full integration of high spectral and high spatial resolution data. Thus the system may represent not only an important innovation in scientific theory but may also contribute to the development of practical field imaging spectrometer products in China. This paper has introduced the basic principle of the FISS, describing its structural design and main technology parameters. Geometric correction, spectral calibration, and laboratory absolute radiometric calibration for the FISS were achieved. In addition, a look-up table of absolute radiometric calibration coefficients was established under a variety of measurement conditions. Based on the results from the FISS prototype, various indoor and in-field tests were carried out for typical features of different regions. The experiments obtained many spectral imaging data for different objects, such as crops, weeds, roads, water, milk, and corn seeds. The results were studied and in each case showed the success of the FISS.

The combined “image and spectrum” imaging mode of the FISS greatly improves working efficiency and discrimination, especially in comparison to traditional point-record field spectrometers. Compared with airborne imaging spectrometers, the FISS can acquire higher spatial resolution images from which a relatively pure pixel may be extracted, which may aid in analyzing mixture spectra and modeling and provide a new solution for classification, discrimination, and target component estimation. Therefore, as future research, we will focus on studying mixed spectra, analyzing the spectral composition of pixels under various scales, and developing a mixed pixel model based on the FISS. To ensure that research based on the FISS advances, all parameters should be adjusted or improved according to the latest developments both in China and abroad.

REFERENCES

Borregaard T, Nielsen H, Norgaard L and Have H. 2000. Crop-weed discrimination by line imaging spectroscopy. *Journal of Agricultural Engineering Research*, **75**(4): 389

Fang J Y, Qi H X, Liu X, Xue Y Q, Zhen L F and Tong Q X. 2009. The principle and experiments of a new field imaging spectrometer. Proceedings of the 7th Technology and Application of Imaging Spectroscopy

Green R O, Eastwood M L and Sarture C M. 1998. Imaging spectroscopy and the airborne visible/infrared imaging spectrometer (AVIRIS). *Remote Sensing of Environment*, **65**(3): 227—248

Huang W J, Wang Q P, Ma Z H, Sun G and Wang J H. 2009. Agricultural field imaging spectrometer development and its applications. Proceedings of the 7th Technology and Application of Imaging Spectroscopy

Li Q C and, Jiang Y J. 1999. The Principle of Spectrometer. Beijing: Beijing Institute of Technology Press

Liu B, Fang J Y, Liu X, Zhang L F, Zhang B and Tong Q X. (To be published) Research on crop-weed discrimination using a field imaging spectrometer. *Spectroscopy and Spectral Analysis*

Liu Y N, Xue Y Q, Wang J Y and Shen M M. 2002. Operational modular imaging spectrometer. *Journal of Infrared and Millimeter Waves*, **21**(1): 9—13

Monteiro S T, Minekawa Y, Kosugi Y, Akazawa T and Oda K. 2007. Prediction of Sweetness and amino acid content in soybean crops from hyperspectral imagery. *ISPRS Journal of Photogrammetry & Remote Sensing*, **62**: 2—12

Theodoridis S and Koutroumbas K. 2006. Pattern Recognition. Beijing: China Machine Press

Tong Q X, Zhang B and Zhen L F. 2006. Hyperspectral Remote Sensing. Beijing: Higher Education Press

Wang S and Xu K X. 2006. Study of preprocessing of near infrared spectral data of milk constituent. *Infrared*, **27**(11): 27—30

Ye X J, Sakai K, Okamoto H and Garciano L O. 2008. A Gound-based hyperspectral imaging system for characterizing vegetation spectral features. Computers and Electronics in Agriculture, **63**: 13—21

Zhang L P and Zhang L F. 2005. Hyperspectral Remote Sensing. Wuhan: Wuhan University Press

地面成像光谱辐射测量系统及其应用

童庆禧[1], 薛永祺[2], 王晋年[1], 张立福[1], 方俊永[1], 杨一德[2], 刘 学[1], 亓洪兴[2], 郑兰芬[1], 黄长平[1]

1.中国科学院 遥感应用研究所 遥感科学国家重点实验室, 北京 100101;
2.中国科学院 上海技术物理研究所, 上海 200083

摘 要: 系统介绍了自主研制的基于制冷面阵 CCD 地面成像光谱辐射测量系统(field Imaging spectrometer system, FISS)的成像原理, 结构设计, 主要指标参数和数据处理流程等。利用室内布设的精确标志点和野外测量数据纠正了 FISS 系统几何畸变; 利用自行开发的光谱定标软件对 FISS 系统进行波长定标, 确定了各通道中心波长和全波半高宽; 在室内, 以积分球为光源, 对 FISS 系统逐波段进行了绝对辐射定标, 定标精度优于 5%, 并建立了各种测量条件下绝对辐射定标系数查找表; 最后, 利用 FISS 系统样机进行了大量室内和野外测量实验, 并基于获取的部分数据做了作物-杂草识别、近海岸海洋环境试验、牛奶品种识别和植物生化参量反演等研究。研究结果表明, FISS 系统能够成功地用于上述领域的研究, 并在地质、食品、农业、林业和城市等领域也具有强大的应用潜力。

关键词: 高光谱遥感, 成像光谱仪, 地面成像光谱辐射测量系统, 系统设计, 遥感应用

中图分类号: TP702 **文献标识码:** A

引用格式: 童庆禧, 薛永祺, 王晋年, 张立福, 方俊永, 杨一德, 刘 学, 亓洪兴, 郑兰芬, 黄长平. 2010. 地面成像光谱辐射测量系统及其应用. 遥感学报, **14**(3): 409—422

Tong Q X, Xue Y Q, Wang J N, Zhang L F, Fang J Y, Yang Y D, Liu X, Qi H X, Zheng L F and Huang C P. 2010. Development and application of the field imaging spectrometer system. *Journal of Remote Sensing*. **14**(3): 409—422

1 引 言

成像光谱技术将传统的二维成像遥感技术和光谱技术结合在一起, 使其能同时获得地物的图像和光谱数据, 具有“图谱合一”的重要特性。成像光谱仪的出现解决了传统科学领域“成像无光谱”和“光谱不成像”的历史问题(童庆禧等, 2006; 张良培等, 2005)。目前中国航空成像光谱技术比较成熟, 取得了一系列重大突破和应用成果, 在世界航空成像光谱中占据重要地位(刘银年等, 2002)。

航空成像光谱仪获取的图谱数据空间分辨率可达几米到几十米(Green 等, 1998), 只能从宏观上监测和评价地物, 由于观测尺度、角度和周围环境背景等影响, 从图像上提取的光谱并不是纯的单一地物的光谱, 基于此混合光谱的后续分析应用也会带来一定的偏差。为了深入地物目标的微观世界, 增加目标的解析率, 减少周围环境背景对地物目标的光谱影响, 提高光谱测量的稳定性和准确性, 促进国内有关地面波谱测量和航空成像光谱技术的进一步发展和完善, 中国科学院遥感应用研究所和上海技术物理研究所以中国自行研制的航空推扫成像光谱仪 PHI 为原型, 联合研制了地面成像光谱辐射测量系统(field imaging spectrometer system, FISS)。FISS 通过地面测量既可获取测量目标的高分辨率图像(空间分辨率可达厘米甚至毫米级)又能获得图像上任意点的光谱曲线, 既提高了野外地面光谱测量的工作效率, 又为目标的结构光谱分析、混合光谱分解和纯像元提取工作提供了更有利的信息数据。与传统地面光谱辐射计相比, FISS 获取的光谱可认为是纯光谱, 有利于混合光谱研究和可变尺度下的像元光谱组构分析。

地面成像光谱仪器设备在国外起步较早, 并

收稿日期: 2010-03-04; 修订日期: 2010-03-11

基金项目: 中国科学院重大科研装备研制项目(地面成像光谱辐射测量系统研制), 国家 863 重点项目(编号: 2008AA121102, 2008AA121103)和国家科技支撑计划项目(编号: 2007BAH15B01)。

第一作者简介: 童庆禧(1935—), 男, 中国科学院院士, 国际欧亚科学院院士, 研究员, 博士生导师, 遥感技术与应用专家, 倡导和发展了高光谱遥感技术和应用研究, 发表论著 70 余篇。 E-mail: tqxi@263.net。

取得了诸多应用成果(Borregaard 等，1999；Ye 等，2008; Monteiro 等, 2007)。目前国外很多公司和研究机构专门从事这种设备的研制，如芬兰的 Spectral Imaging Ltd.公司，美国的 Resonon 和 Surface Optics Corporation 公司等。但在国内尚无先例，本文提出的基于制冷面阵 CCD 的 FISS 系统的研制属于针对遥感基础研究领域的科学仪器原始创新，研制过程中关键技术的突破也将加强中国在探测器技术、成像光谱技术、光谱分光技术、高速采集和存储技术等方面的技术发展，提高自主创新能力。

2 FISS 系统设计和实现

2.1 设计基本原理

FISS 的设计借鉴和参照了中国自行研制的航空推扫成像光谱仪 PHI 的设计原理，对成像系统、分光系统和控制软件进行改进和重新设计。其成像原理与 PHI 类似：沿狭缝方向一维形成空间像；垂直于狭缝一维为空间各像元的光谱，由色散元件得到；数据的另一空间维由扫描镜完成(方俊永等，2009；李全臣等, 1999)。

图 1 是 FISS 原理图，地物通过一个垂直于轨道方向的狭缝成像，其光线经过准直镜后平行射出，经色散器件在垂直条带方向按光谱色散，经过会聚镜成像在探测器的光敏面上，光敏面水平行像元(平行于狭缝，称空间维)对应地物条带的每个波段影像；垂直列像元(色散方向，称光谱维)对应地物条带的空间采样视场光谱色散的影像。对每个地物条带，面阵探测器会生成一帧光谱图像数据；再加上扫描镜在一定角度范围内的扫描和一定的记录速率，就可以连续记录光谱图像，得到“图谱合一”的图像立方体。

2.2 结构设计

FISS 主要有 3 个系统构成，即：计算机系统、光机系统和电子学系统。

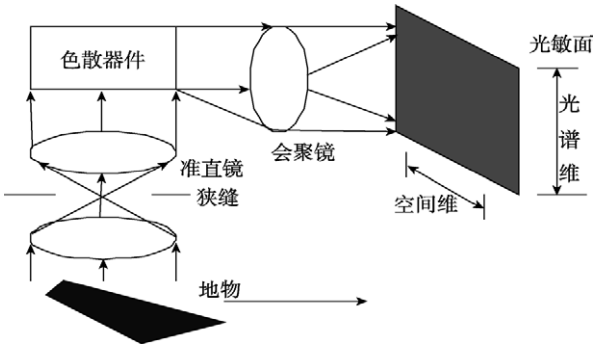

图 1 FISS 原理图

计算机系统包括硬件和软件：硬件是一台便携式笔记本电脑，用来实时监控和存贮图谱数据和其他辅助数据；软件是用来操作 FISS 系统的计算机程序和基本数据处理分析软件。

光机系统是 FISS 的核心部分，由扫描镜、光学镜头、分光器件和 CCD 相机等组成，图 2 是研制成功的 FISS 光机系统实物图。

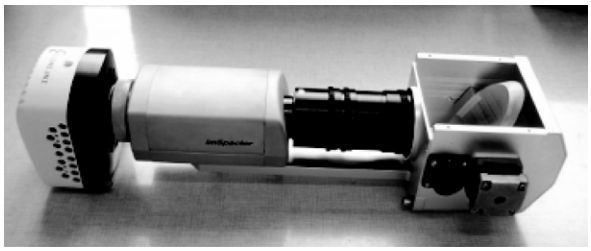

图 2 FISS 光机系统实物图

光机系统完成空间扫描、成像、色散、光电转换和 A/D 转换等功能。扫描镜主要由椭圆反射镜、步进电机及其机械框架组成，扫描镜在步进电机的驱动下在一定角度范围内来回摆动，实现对地物空间一维的扫描；光学镜头将地面目标清晰的呈现在分光器件的入射狭缝上，其焦距和狭缝宽度决定了仪器垂直运动方向上成像的空间分辨率；分光器件采用“棱镜-光栅-棱镜”组合系统(即 P-G-P 系统)分散通过入射狭缝的光能量，并会聚在 CCD 相机的光敏面上，分光器件决定了 FISS 系统的波段数量和光谱分辨率；面阵 CCD 相机(型号为 INFINITY3-1)将接收到的光信号转换为电信号，决定了获取影像的清晰度，即能否有效的达到光学部分决定的空间和光谱分辨率。

电子学系统主要包括电源和电机控制电路。电源主要为 CCD 相机供电，采用摄像机用锂电池；电机控制电路主要负责接收计算机的控制指令以驱动电机的运转，控制电路通过 USB 接口和计算机通讯，并从 USB 口取电。

为便于野外测量，设计了坚固耐用、拆卸简单、结构紧凑、移动灵活、架设方便的地面测量多用途工作平台，其中，高强度的支架及旋臂采用三角形稳定性的结构设计，并采用转轴和插销的方式实现旋臂的旋转和固定，采用直线和环形刻度盘提供旋臂的位置和角度参数。图 3 为完整的 FISS 系统构成示意图。

多用途平台由三脚架和精密导轨构成，用于承载光机系统和电子学系统，并可通过精密导轨实现测量长度调节和水平面内的 360°旋转测量，配备高精度 GPS 后可提供精确的定位信息，图 4 是 FISS 野外测量示意图和实际测量工作图。

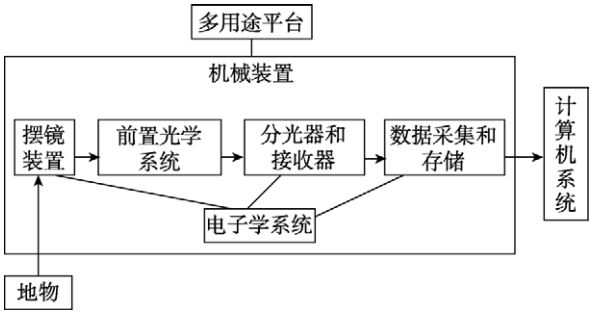

图 3 FISS 构成示意图

2.3 FISS 主要技术指标

FISS 主要指标参数包括光谱范围、光谱分辨率、空间分辨率和帧速率等，表 1 列举了 FISS 系统的主要指标参数和性能。

2.3.1 光谱范围和光谱分辨率

FISS 系统的光谱范围取决于分光器件和 CCD 相机的光谱响应范围。CCD 传感器的光谱响应在 400—1000nm, ImSpector V9 分光器件的光谱响应为

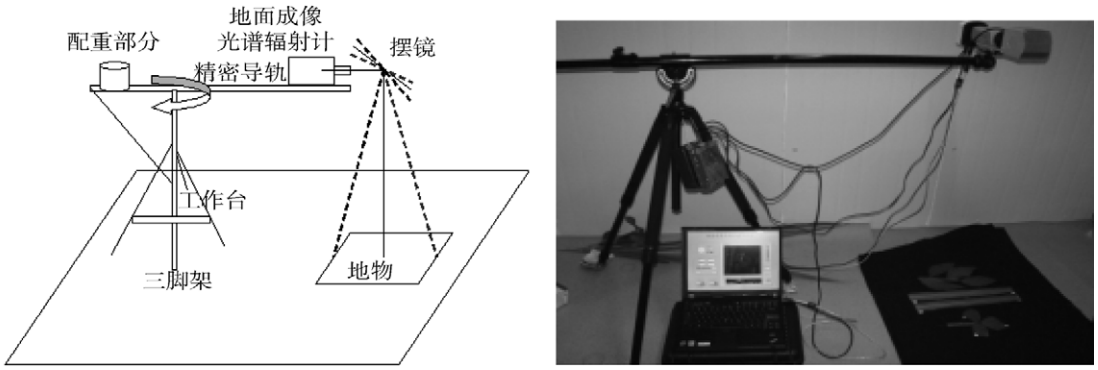

图 4 FISS 野外测量示意图和实际测量工作图

表 1 FISS 系统的主要参数指标和性能

波段数/个	344
光谱范围/nm	379—870
光谱分辨率/nm	4—7
地面分辨率/mm	最高可优于 2
实验室辐射定标精度/%	优于 5
成像速率/(帧/s)	最高 20
扫描视场/(°)	–20—20
量化位数/位	12
信噪比	60%波段>500
光谱采样间隔/nm	约 1.4

430—900nm, FISS 的光谱范围主要由分光器件的光谱响应范围决定。在实验室利用单色仪对本系统进行了波长定标，定标结果表明在 420—860nm 范围内该仪器能很好地响应单色仪发出的光。

FISS 系统的光谱分辨率由分光器件的入射狭缝和 CCD 传感器的光敏元尺寸决定。分光器件入射狭缝宽度 60μm, CCD 传感器分辨率为 1392×1040，为了满足系统的信噪比要求，将像元作 3×3 像元合并变为 464×344，其中空间维是 464，光谱维是 344，即 FISS 具有 344 个光谱通道，此时光敏元大小约为 20μm。采用 1 1 成像机制，光谱分辨率主要由入射狭缝宽度决定，并用光谱通道的半高宽表示。

2.3.2 空间分辨率

FISS 空间分辨率需考虑平行于分光器件入射狭缝方向和垂直于入射狭缝方向。平行于入射狭缝方向上的空间分辨率取决于 CCD 相机焦平面上成像单元的尺寸和光学成像镜头的焦距，用公式表示为

$$\beta=d/f \tag{1}$$

垂直于入射狭缝方向上的空间分辨率取决于狭缝宽度和光学成像镜头的焦距，用公式表示为

$$\alpha=w/f \tag{2}$$

式中，β为平行于入射狭缝方向上的视场角，d 为成像单元的尺寸，α为垂直于入射狭缝方向上的视场角，w 为狭缝宽度，f 为光学成像镜头的焦距。

2.3.3 帧速率

帧速率一般取决于 CCD 相机的数据传输速率和数据采集模式。FISS 系统中 CCD 相机采用 USB 接口传输数据，12 位数据采样。为避免流模式(摄像机模式)采集数据与步进电机无法同步而导致图像模糊，FISS 采用拍照模式(照相机模式)进行数据采集，步进电机每步进一步，发出同步信号触发相机拍照一次。拍照模式下 CCD 相机的帧速率最大为 20 帧/s，野外实验一般设置为 10 帧/s。

3 FISS 系统数据处理

在具体应用前，需要对 FISS 获取的原始数据进行一系列的处理，包括数据格式转换、几何纠正、辐射纠正(辐射定标)、图像分割、截取与拼接，以及针对具体应用做的处理等。图 5 为 FISS 系统数据处理流程图。

3.1 几何纠正

FISS 系统利用反射镜在一定角度范围内摆动代替飞行平台的运动获取地物其中一维的空间信息，地物目标不是同时成像。扫描镜摆扫过程中成像距离的不同造成不同列之间分辨率分布不均匀，引起几何畸变；并且摆镜运动稳定性的差异也会引起不同行之间的分辨率差异。为了纠正这些几何形变，需要精确测定镜头畸变、布设精确标志点、确定几何纠正模型等。为验证和校准扫描镜的平稳性和匀速性，在布设精确标志点时，应布设连续标志点，得到的几何形变信息也为电机的控制提供参考。图 6 为 FISS 系统几何纠正的具体处理流程和实验室内用于几何纠正的精确标志点。

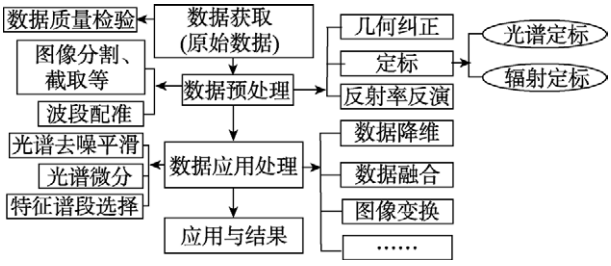

图 5 FISS 系统数据处理流程图

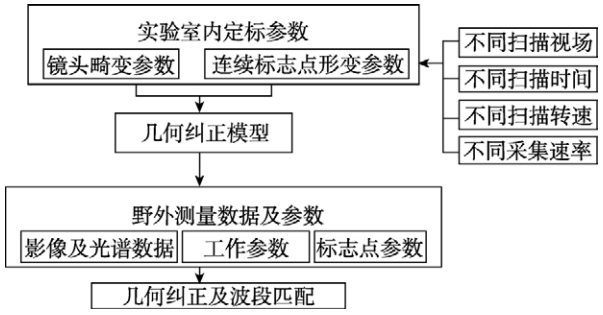

图 6 FISS 系统几何纠正处理流程

利用上述标志点，基于多项式几何校正模型解算出系统变形参数，进而利用变形参数校正 FISS 获取的数据。

3.2 光谱定标

FISS 光谱定标主要采用室内定标的方法，以确定中心波长和半高全波宽度。在实验室利用北京光学仪器厂研制的 WDG30-2 单色仪，采用自行开发的光谱定标软件对 FISS 系统进行波长定标。定标结果给出了不同波长对应的光谱通道带宽和 344 个通道所对应的中心波长。表 2 为光谱响应较好的 420—860nm 波长对应的光谱通道带宽。

3.3 辐射定标

FISS 系统辐射定标采用实验室绝对定标与野外现场相对定标相结合的方法。实验室绝对辐射定标使用已标定的积分球作为光源照射传感器整个视场，并逐波段进行辐射定标(童庆禧等, 2006)。为了满足应用需求，通过改变积分球的辐亮度(控制积分球内标准灯的亮暗数量，共设 8 个等级)、改变光学镜头的光圈大小、积分时间、CCD 制冷温度等条件，建立 FISS 入瞳处输入辐射亮度与数字化输出之间的定量关系 $L_e=a\times DN+b$ (其中 L_e 为入瞳处辐射亮度，DN 为数字化输出值)，并通过线性拟合解得 a 和 b，即为各种温度、光圈和积分时间下仪器各波段的定标系数，建立不同测量条件下 FISS 系统绝对辐射定标系数查找表。图 7(a)为 FISS 系统光学镜头光圈设为 11、CCD 制冷温度为 0℃、积分时间 5ms 时波段 30(中心波长 417.5nm)的定标结果，横坐标为 DN 值，纵坐标为对应的入瞳处辐亮度值，图中直线为线性回归拟合直线，散点为实际测量值。在定标系数查找表中查找波段 30 的定标系数为 a=0.058063，b=−0.30929；定标精度为 3.6%；图 7(b)为同样测量条件下 344 个光谱通道的定标精度。

由图 7(b)可知，大部分波段的辐射定标精度优于 5%，尤其在波段号 32—338(即 420—860nm)内的定标精度远远优于 5%，满足实验室绝对辐射定标精度要求。

野外现场相对定标是指 FISS 在野外测量时先测量一块已知辐射亮度值的参考板后再去测量地面目标，通过参考板来实现标定。

表 2 **420—860nm** 波长对应的光谱通道带宽

波长/nm	420—470	475—625	630—715	720—820	825—860
对应的光谱通道宽度/nm	7	4	5	6	7

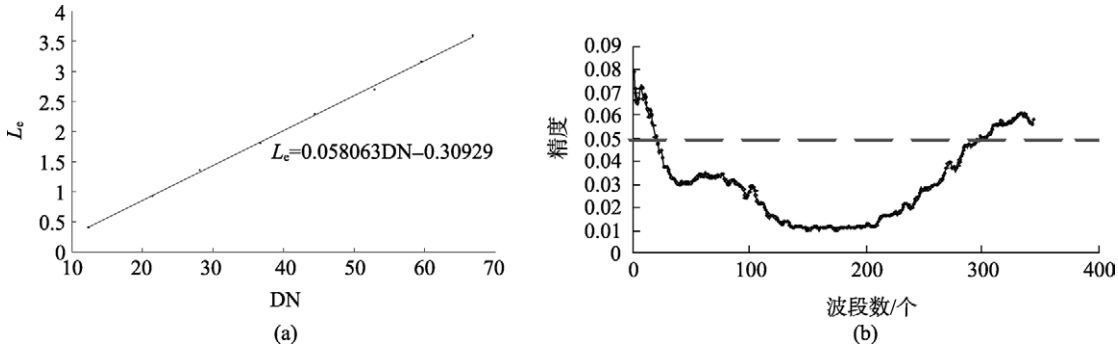

图 7 实验室绝对辐射定标结果

(a) 波段 30(中心波长 417.5nm)的辐射定标结果; (b) 光圈为 11，温度 0℃，积分时间为 5ms 情况各波段的定标精度

4 FISS 系统初步应用结果

利用研制成功的 FISS 系统样机，进行了大量室内和野外实验，采集各种目标成像高光谱数据并调试系统。图 8 为 FISS 系统野外测量工作照。

图 8 FISS 系统野外测量工作照

4.1 室内牛奶光谱测量实验

利用自行研制的 FISS 系统和美国 SVC 公司研制的 HR-1024 辐射仪，在室内以卤素灯为光源的环境下，对超市购买的伊利、蒙牛、光明、三元等 12 种牛奶样品同时测量，并采用 SAM(光谱角填图)、SFF(光谱特征拟合)和 BE(二进制编码)3 种方法分析比较了二者获得光谱数据的差异，旨在证实 FISS 系统实际工作性能的稳定性和准确性及其对地物光谱的响应能力。图 9 是 FISS 获取的牛奶“立方体”数据，每个像元均可提取出一条连续的光谱曲线；图 10 为利用 SAM、SFF 和 BE 3 种方法联合评价 FISS 数据光谱响应性能的结果，三者权重各占 1/3，结果表明 FISS 与 SVC 数据匹配精度超过 97%，说明 FISS 系统光谱响应性能良好，为 FISS 的后续应用研究提供了理论依据和基本保障。

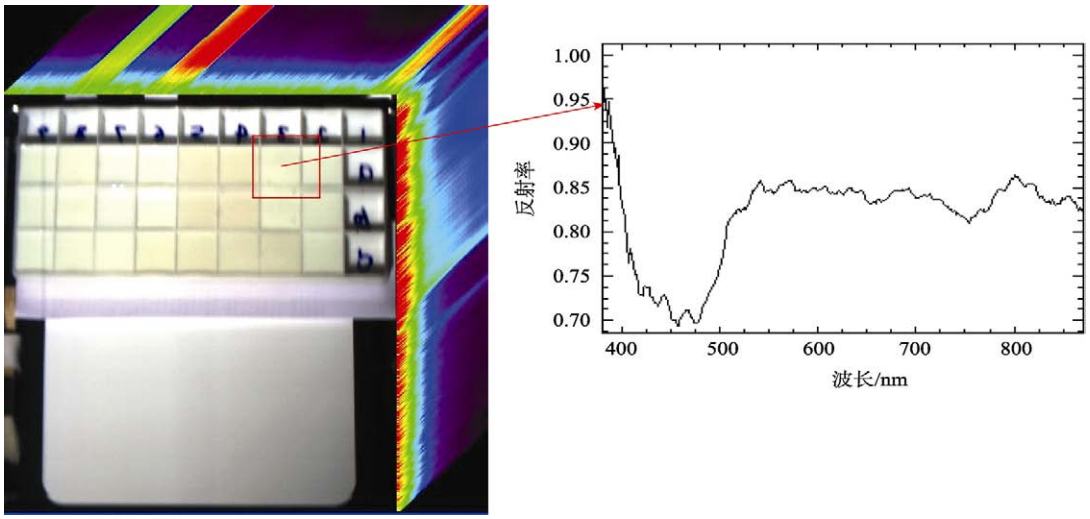

图 9 FISS 获取牛奶的“图谱合一”数据

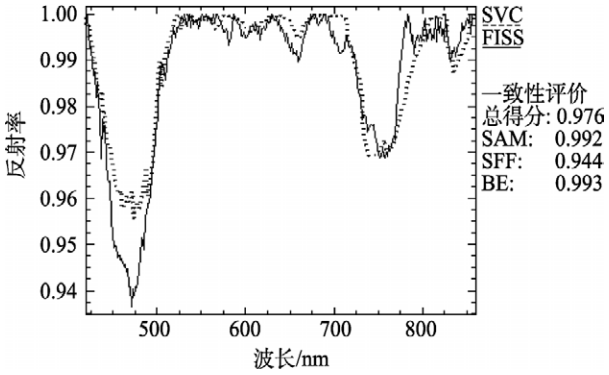

图 10 FISS 与 SVC HR-1024 同步数据匹配

同时对 FISS 获取的牛奶高光谱数据随机取样，每种牛奶取 100 个像元样本，对所有样本光谱做一阶微分和移动平均平滑等预处理(王硕等，2006)，利用 Wilks'lambda 逐步判别分析法选择了 12 个特征波长，采用 Fisher 线性判别法识别不同品种的牛奶，12 种牛奶的总体正确识别率达到 94.1%，其中蒙牛原味酸牛奶、伊利原味酸牛奶等正确识别率高达 100%，即能完全识别出。

4.2 作物杂草识别

采用同样的方法(Fisher 线性判别法)，对在自然环境下，在北京大兴区务各庄农田利用 FISS 系统获取的胡萝卜幼苗以及马齿苋、牛筋草和地锦等杂草的高光谱数据做采样、归一化等处理，并进行了识别(刘波等，待刊)。结果表明，每种杂草单独作为一类加以区分时，利用 8 个特征波段建立模型对杂草和胡萝卜的识别率达 85%左右；而所有杂草作为一类与胡萝卜进行区分时，利用 7 个特征波段识别率高于 91%。研究还发现，红边波段对杂草有显著的识别能力。图 11(a)为 FISS 获取的作物-杂草“立方体”数据，图 11 (b)为杂草识别结果。

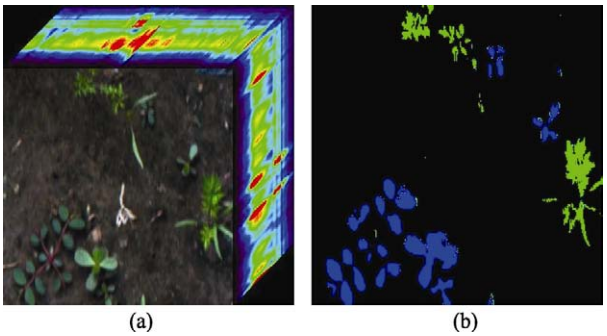

图 11 作物-杂草识别

(a) 作物-杂草“立方体”数据; (b) 杂草识别结果

4.3 植物叶片生化信息反演

叶绿素和氮素作为植物重要的生化参量，指示植物的生物化学状态，为作物精准施肥等应用提供了重要信息。2009 年 8 月，在中国科学院广西环江喀斯特生态环境实验站，利用 FISS 系统和传统点测量仪 ASD 同步采集了 102 个大豆叶片样本的高光谱数据。对大豆光谱数据做预处理，剔除异常样本等，建立了大豆叶片叶绿素和 N 含量反演模型。结果表明，FISS 的“图谱合一”数据能够定量反演大豆叶片生化参量，将大豆叶片图像偏差和均值数据混合建立偏最小二乘回归模型，其预测精度超过 95%；与传统点测量 ASD 数据相比，FISS 预测叶绿素和 N 含量的精度更高。表 3 为利用主成分回归(PCR)和偏最小二乘回归(PLSR)建立反演大豆叶绿素模型的结果，与 ASD 数据相比，FISS 数据建模预测精度分别提高了 33%和 42%。

表 3 **FISS** 和 **ASD** 数据反演结果比较

	FISS		ASD	
	预测误差	预测可决系数	预测误差	预测可决系数
PCR	0.272332	0.873925	0.405452	0.720781
PLSR	0.236337	0.95001	0.406416	0.84673

4.4 近海岸的海洋环境试验

2009-11-28，利用 FISS 系统进行了海洋环境的试验。将 FISS 载于 30m 的高架车上获取了青岛近海岸的海洋环境高分辨率成像光谱数据。通过对 FISS 成像光谱数据的分析，获取了高分辨率青岛近海岸的海水叶绿素分布、海水浑浊度、海水污染分布等重要数据，其目的是通过遥感定量反演模型，进一步定量分析海水叶绿素浓度、海水浑浊度、污染分布等范围。经过初步分析，证明 FISS 对于以上问题的研究是很有效的，具有重要应用价值。

5 总结与展望

自主研制的地面成像光谱辐射测量系统(FISS)在测量地物光谱时能同步实现高分辨率成像，实现高光谱和高空间分辨率数据的完全融合，这不仅是在科学理论上的重要创新，也是推动中国实用型地面成像光谱产品的快速发展。本文详细介绍了 FISS 系统的基本原理、结构设计和主要技术指标参数，并对 FISS 系统作了精确的几何纠正、光谱定标和实

验室绝对辐射定标，建立了各种测量条件下的绝对辐射定标系数查找表。基于研制成功的 FISS 系统样机，针对不同区域典型地物进行了室内和野外成像光谱测量及系统调试，获得了作物、杂草、路面、水体、牛奶、玉米种子等多种物质的成像光谱数据，利用获取的数据做了相关研究，取得良好成果。

FISS 从本质上改变了传统地面光谱仪点测量方式，“图谱合一”成像模式，大大提高了工作效率；与航空成像光谱仪相比，FISS 具有更高的空间分辨率，可以提取非常纯的像元，有利于混合光谱及解混的分析和模型建立，为地物分类和识别、地物目标组分反演提供了新的解决途径。因此，基于 FISS 系统的混合光谱研究、可变尺度下的像元光谱组构分析和混合像元模型发展是今后的主要研究工作之一；同时为了保证研究成果的先进性，必须参考最新发展，对 FISS 系统总体指标进行调整或修正等。

REFERENCES

Borregaard T, Nielsen H, Norgaard L and Have H. 2000. Crop-weed discrimination by line imaging spectroscopy. *Journal of Agricultural Engineering Research*, **75**(4): 389

Fang J Y, Qi H X, Liu X, Xue Y Q, Zhen L F and Tong Q X. 2009. The principle and experiments of a new field imaging spectrometer. Proceedings of the 7th Technology and Application of Imaging Spectroscopy

Green R O, Eastwood M L and Sarture C M. 1998. Imaging spectroscopy and the airborne visible/infrared imaging spectrometer (AVIRIS). *Remote Sensing of Environment*, **65**(3): 227—248

Huang W J, Wang Q P, Ma Z H, Sun G and Wang J H. 2009. Agricultural field imaging spectrometer development and its applications. Proceedings of the 7th Technology and Application of Imaging Spectroscopy

Li Q C and, Jiang Y J. 1999. The Principle of Spectrometer. Beijing: Beijing Institute of Technology Press

Liu B, Fang J Y, Liu X, Zhang L F, Zhang B and Tong Q X. (To be published) Research on crop-weed discrimination using a field imaging spectrometer. *Spectroscopy and Spectral Analysis*

Liu Y N, Xue Y Q, Wang J Y and Shen M M. 2002. Operational modular imaging spectrometer. *Journal of Infrared and Millimeter Waves*, **21**(1): 9—13

Monteiro S T, Minekawa Y, Kosugi Y, Akazawa T and Oda K. 2007. Prediction of Sweetness and amino acid content in soybean crops from hyperspectral imagery. *ISPRS Journal of Photogrammetry & Remote Sensing*, **62**: 2—12

Theodoridis S and Koutroumbas K. 2006. Pattern Recognition. Beijing: China Machine Press

Tong Q X, Zhang B and Zhen L F. 2006. Hyperspectral Remote Sensing. Beijing: Higher Education Press

Wang S and Xu K X. 2006. Study of preprocessing of near infrared spectral data of milk constituent. *Infrared*, **27**(11): 27—30

Ye X J, Sakai K, Okamoto H and Garciano L O. 2008. A Gound-based hyperspectral imaging system for characterizing vegetation spectral features. Computers and Electronics in Agriculture, **63**: 13—21

Zhang L P and Zhang L F. 2005. Hyperspectral Remote Sensing. Wuhan: Wuhan University Press

附中文参考文献

方俊永，亓洪兴，刘学，薛永祺，郑兰芬，童庆禧. 2009. 地面成像光谱辐射计的设计和初步结果.第七届成像光谱技术与应用研讨会文集

黄文江，王秋平，马智宏，孙刚，王纪华. 2009. 农业田间成像光谱仪的研制与应用. 第七届成像光谱技术与应用研讨会文集

李全臣，蒋月娟. 1999. 光谱仪器原理.北京：北京理工大学出版社

刘波，方俊永，刘学，张立福，张兵，童庆禧. 基于成像光谱技术的作物杂草识别研究(待刊). 光谱学与光谱分析

刘银年，薛永祺，王建宇，沈明鸣. 2002. 实用型模块化成像光谱仪，红外与毫米波学报. **21**(1): 9—13

童庆禧，张兵，郑兰芬. 2006. 高光谱遥感——原理、技术与应用. 北京：高等教育出版社

王硕，徐可欣. 2006. 牛奶成分近红外光谱数据的预处理研究. 红外, **27**(11): 27—30

张良培，张立福. 2005. 高光谱遥感. 武汉：武汉大学出版社